Jurnal Kejuruteraan 38(1) 2026: 455-463
https://doi.org/10.17576/jkukm-2026-38(1)-39

Design and Experimental Study of Shape Memory Alloy (SMA) Spring as Actuators in Wrist Exoskeleton

Azni Nabela Wahid* & Muhammad Hadif Badarussamin

Department of Mechatronics Engineering, Kulliyyah of Engineering, International Islamic University Malaysia

**Corresponding author: azni@iium.edu.my*

Received 1 July 2025, Received in revised form 30 September 2025
Accepted 30 October 2025, Available online 30 January 2026

ABSTRACT

This paper presents the design, modeling, and experimental assessment of a wrist exoskeleton actuated by Shape Memory Alloy (SMA) springs to support flexion-extension and radial-ulnar deviation of the wrist. A dynamic model based on the Euler-Lagrange formulation was developed and simulated to estimate the joint torque requirements, which ranged from 0.26–0.32 Nm for standard wrist movements. A prototype is fabricated and tested incorporating four SMA spring actuators fixed on an arm splint, with targeted actuation for generating different wrist motion. Experimental findings revealed that the prototype delivered torque values surpassing simulation requirements for flexion (0.332 Nm) and extension (0.328 Nm) motions, whereas lower torque was observed for radial and ulnar deviations, likely due to actuator placement and frictional losses. The actuation cycle frequency for flexion-extension was measured to be 0.018 Hz, primarily constrained by the thermal characteristics of the SMA springs. Another important observation is enhanced speed during SMA reversal motion (from extension to flexion) resulted from antagonistic actuation of the SMA. To further improve the torque and speed generation, an optimal SMA actuator with reduced thermal mass (thinner diameter, bundle configuration) and active cooling can be designed. Overall, the SMA-driven wrist exoskeleton exhibits promising potential as a lightweight, wearable system for effective wrist joint assistance.

Keywords: Shape memory alloy; actuator; artificial muscle; wrist exoskeleton; flexion-extension; radial-ulnar deviation

INTRODUCTION

Robotic exoskeletons are a remarkable innovation in assistive technology, providing mechanical support to individuals with muscle weakness or neurological disorders. They are generally divided into two types: rigid and soft, each with its own pros and cons, such as differences in load capacity and speed (Yeem et al. 2019). These robots use different actuators (hydraulic, electric, and pneumatic) and control methods, which greatly affect their performance. However, these traditional actuator systems often face significant challenges due to their bulkiness and weight, which can compromise user comfort and practicality, especially in wearable devices where ease of movement and lightness are crucial (Villena et al. 2019).

RELATED WORKS

Traditional wrist rehabilitation devices commonly employ electric, pneumatic, or hydraulic actuators. For instance, Krebs et al. (2007) pioneered early robotic systems that utilized electric motors for precise wrist rehabilitation exercises. While effective, these systems were often bulky and expensive, limiting their use to clinical environments. Similarly, Zhang et al. (2020) introduced a Parallel Wrist Rehabilitation Robot (PWRR) that used electric actuators to enhance motion accuracy and mechanical rigidity. Though the design showed improved motion control, it still suffered from a large physical footprint. Pneumatic actuators have also been explored for their compliance and safety in physical human-robot interaction. Wang and Xu

(2021) developed a soft parallel robot based on pneumatic artificial muscles (PAMs) however, the requirement of air compressor added complexity. Likewise, Su et al. (2019) proposed a compact wrist rehabilitation robot with advanced force and stiffness control using precise actuator systems, though the authors acknowledged the challenges related to misalignment and size. Mayetin and Kucuk (2021) proposed a 3-DOF force-sensing unit to support better feedback control in wrist rehabilitation, but the inclusion of force sensors and rigid actuators further added bulkiness to the system.

A comprehensive review by Garcia et al. (2024) summarized the state-of-the-art in wrist rehabilitation robots and highlighted the persistent issues of bulkiness and lack of adaptability in existing systems. The review emphasized the need for innovative actuation technologies to create lighter, more wearable, and user-friendly devices. SMA materials, which change shape in response to temperature changes, offer a promising solution as actuators. They are known for their high energy density, flexibility, and light weight, making them ideal for use in robotic exoskeletons (Hamid et al. 2023; Pittaccio et al. 2012; Tang et al. 2013). Simone et al. (2020) emphasized their suitability in soft robotic hands, showing SMA wires embedded in fingers could produce significant grasping forces while maintaining flexibility. To overcome SMA strain limitations, Park et al. (2020) developed a Shape Memory Alloy Spring Bundle Actuator (SSBA) enclosed in silicone tubing and actuated by temperature-controlled water. The system, bundling 24 springs, demonstrated scalable force output (up to 10 kg load) and significant displacement gains when heated. Park et al. (2020) proposed a SMA Fabric Muscle (SFM) integrating 20 SMA springs into fabric layers through stitching. The actuator achieved a minimum force of 100 N and 50% contraction strain. Its textile nature allowed seamless integration into wearable garments, offering comfort and compliance. Jeong et al. (2019) introduced Soft Wrist Assist (SWA), a wearable robot powered by five SMA spring actuators. Optimized for wrist flexion, extension, and radial/ulnar deviation, the design combined SMA springs with a cooling system in a compact layout, able to deliver up to 10 N force with 40% contraction strain. Ali and Kim (2023) presented a novel artificial muscle using spiral windings of a single SMA wire routed through pulleys and roller bearings. This design extended actuator length without increasing the linear footprint, allowing compact yet strong SMA actuation. Jia et al. (2024) introduced an Artificial Muscle Matrix (AMM) embedded in a Smart Digital Structure (SDS) with NiTi SMA wires and silicone elastomer. This actuator achieved synchronized control of force and displacement with compact dimensions and was intended for bionic joint applications. Hope and McDaid (2017) developed a wrist and forearm exoskeleton actuated by SMA wires with mechanical amplification and rotary sensors. Using differential and bias-spring configurations, they achieved multi-DOF control (pronation-supination, radial-ulnar deviation, and flexion-extension).

While previous research shows SMA actuator's potential in exoskeleton, most designs are either complex or need external cooling system. This work aims to address this gap by presenting the design, modeling, and experimental validation of a simple wrist exoskeleton prototype. The design incorporates four SMA springs in antagonistic configurations to effectively control all four targeted wrist motions i.e. flexion, extension, ulnar and radial deviation; without complex bundling or fluid cooling for enhanced speed.

METHODOLOGY

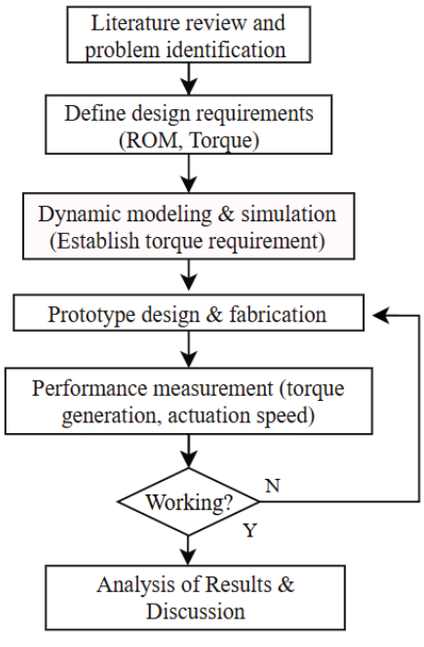

FIGURE 1. Workflow of the research

In this work, the modelling, design and construction of a flexion/extension and radial/ulnar wrist joint rehabilitation device utilizing SMA springs as actuators will be performed and tested. The work starts with simulation studies to estimate the required joint torque during both flexion-extension and ulnar-radial deviation motions. The estimated joint torque from the model will be compared with the torque output of the SMA-based wrist assistive device to assess whether the actuator can deliver sufficient force to achieve the intended movement, and recommendations for further improvement of the prototype.

KINEMATICS OF WRIST ROTATIONS

Understanding the biomechanics of wrist motion is vital for designing effective assistive devices that aim to restore or enhance wrist function. The wrist joint is a highly complex and versatile structure that allows for a wide range of motion, including flexion-extension, ulnar-radial deviation, supination, and pronation. Flexion typically ranges from 60° to 80°, while extension ranges from 60° to 75°. Ulnar deviation, which is the movement of the wrist towards the little finger, ranges from 30° to 45°, and radial deviation, the movement towards the thumb, ranges from 15° to 25° (Parelli et al. 2023; Fischer et al. 2020)

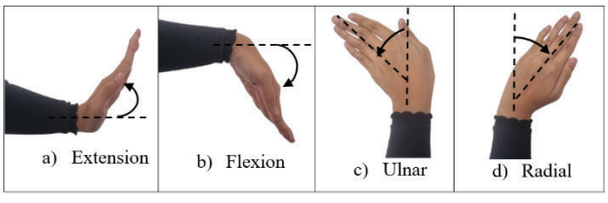

FIGURE 2. Motion of wrist in a) extension b) flexion c) ulnar deviation d) radial deviation

MODELLING AND SIMULATION STUDIES

The dynamic models for wrist joint flexion-extension and ulnar-radial deviation are derived using the Euler-Lagrange formulation where k is the system's DOF, q_k is the set of the generalized coordinates, and Q_k is the set of non-conservative forces (Garcia et al. (2024), Serbest et al. (2018)):

$$\frac{d}{dt}\left(\frac{\partial L}{\partial \dot{q}_k}\right) - \frac{d}{dt}\left(\frac{\partial L}{\partial q_k}\right) = Q_k \tag{1}$$

Lagrangian, L is the difference between kinetic energy, T and potential energy, V of the system:

$$L = T - V \tag{2}$$

Where T and V are taken as:

$$T = \frac{1}{2}ml^2\dot{\theta}^2 + \frac{1}{2}J\dot{\theta} \tag{3}$$

$$V = mgl\sin\theta \tag{4}$$

J is the moment of inertia, θ and $\dot{\theta}$ are angular displacement and velocity, respectively. m is mass and the gravity center is located at a proximal distance, l. From Eq. (1), angle θ is taken as the generalized coordinate, torque and viscous damping; with damping coefficient, c as the non-conservative forces. Therefore, the Euler-Lagrangian model is updated as:

$$\frac{d}{dt}\left(\frac{\partial L}{\partial \dot{\theta}_k}\right) - \frac{d}{dt}\left(\frac{\partial L}{\partial \theta_k}\right) = \tau - c\dot{\theta} \tag{5}$$

Solving the second order ODE, the dynamic models for wrist joint flexion-extension and ulnar-radial deviation can be written as:

$$ml^2\ddot{\theta} + J\ddot{\theta} + mgl\cos\theta = \tau - c\dot{\theta} \tag{6}$$

This model will be simulated using Simulink by solving the highest order derivative as:

$$\ddot{\theta} = \frac{1}{ml^2 + J}\left(\tau - c\dot{\theta} - mgl\cos\theta\right) \tag{7}$$

The parameters used for the dynamic models are tabulated as follows:

TABLE 1. Parameters for dynamic motion of wrist (Thomas et al. 2022)

Parameter for hand	Value
Mass, m (kg)	0.6% of body mass
Length, L (m)	10.8% of body height
Proximal distance, l (m)	50.6% of hand length
Moment of inertia, J (kgm^2)	mk^2
Damping coefficient, c (Nms)	0.01
Radius of gyration, k (m)	29.7% of hand length

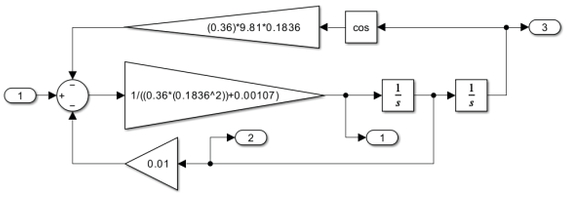

FIGURE 3: MATLAB Simulink model for Eq. 7

For simulation study, parameters shown in Table 1 are used incorporating the average Malaysian adult body mass and height. A closed-loop PID controller was implemented

within the dynamic model. It operates by taking the tracking error i.e. the difference between the desired reference trajectory and the actual angular displacement of the hand as its input and generating the corresponding joint torque as output to drive the movement. This approach enables the estimation of joint torque during both flexion-extension and ulnar-radial deviation motions, across ranges of motion. It also provides a framework for evaluating and selecting appropriate actuators in exoskeleton design. The estimated joint torque from the model is subsequently compared with the torque output of the prototype, presented in the later section.

A Proportional–Integral–Derivative (PID) controller is a widely used control strategy in engineering systems due to its simplicity. The PID controller comprises proportional term (*P*), which produces an output proportional to the current error, *e(t)*, the integral term (*I*), which accounts for the accumulation of past errors to eliminate steady-state error; and the derivative term (*D*), which predicts future error based on its rate of change. Its output *u(t)* is mathematically expressed as:

$$u(t) = K_p e(t) + K_i \int e(t)dt + K_d \frac{de(t)}{dt} \qquad (8)$$

In this study, the PID parameters were determined using a heuristic tuning method. The PID gains which yielded stable and responsive control behavior for the model are found to be $K_p = 100$, $K_i = 3$, and $K_d = 20$.

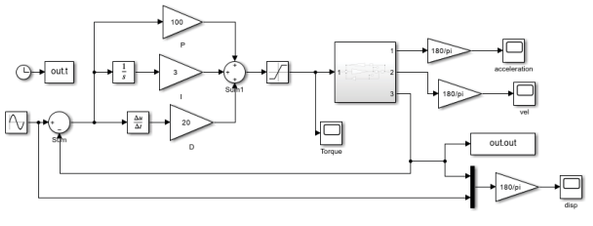

FIGURE 4. MATLAB Simulink model with PID implementation

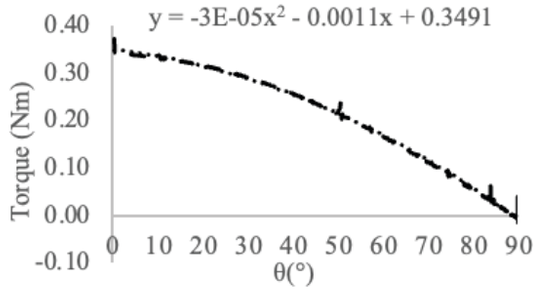

FIGURE 5. Simulation result: Angular displacement vs. time

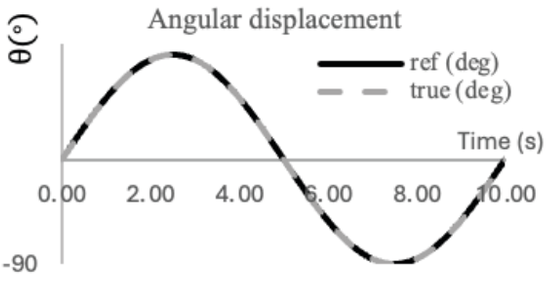

FIGURE 6. Simulation result: Torque vs. time

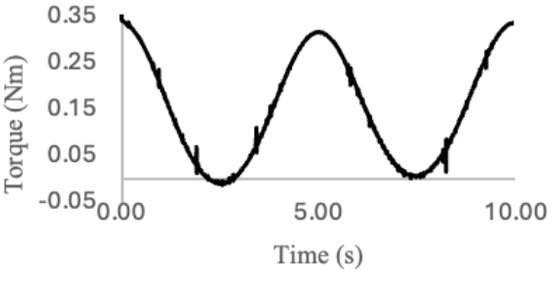

FIGURE 7. Simulation result: Correlation between torque required and wrist angular displacement

The simulation results shown in Figures 5, 6 and 7 demonstrate the performance of the wrist exoskeleton under PID control using dynamic model in Eq (7). In Figure 5, the angular displacement closely tracks the reference trajectory with respect to time. Figure 6 shows the simulated joint torque required to actuate the wrist at different angular position, where maximum torque values recorded are 0.27 Nm for extension, 0.26 Nm for flexion and 0.33 Nm for both radial and ulnar deviations. It can be observed that the maximum torque required occurred at $\theta = 0°$ when the hand is positioned perpendicular to the direction of gravity, where the moment arm is longest. As the hand moves, the torque decreases due to the shortening of the perpendicular distance between the force vector and the joint axis. In Figure 7, the correlation between required torque at different angular displacements of the wrist is shown.

In healthy individuals, the maximum torque generated during daily activities (ADL) ranges from 6–10 Nm for pronation/supination, 8–14 Nm for flexion/extension, and about 1.3 Nm for radial/ulnar deviation. For rehabilitation, lower torque levels are recommended to prevent injury or strain, especially in patients with muscle or bone impairments. Therapeutic guidelines suggest applying torque between 0.35–1.5 Nm for flexion/extension and not more than 0.5 Nm for radial/ulnar deviation (Pitzalis et al. 2023; Serrano et al. 2018). For this study, the ROM targeted for the wrist movements, and the corresponding required torque value obtained from simulation study are shown in Table 2:

TABLE 2. Theoretical required torque and targeted ROM

Motion	TargetROM	Required torque, τ_{req} (Nm)
Extension	30°	0.27
Flexion	40°	0.26
Radial	15°	0.32
Ulnar	20°	0.32

PROTOTYPE DEVELOPMENT

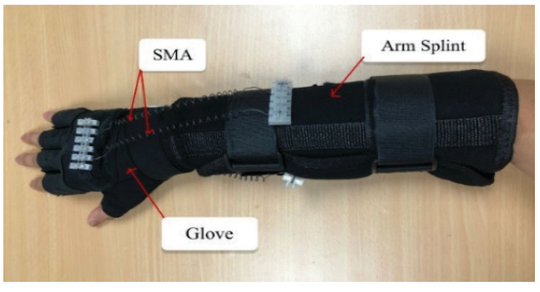

(a)

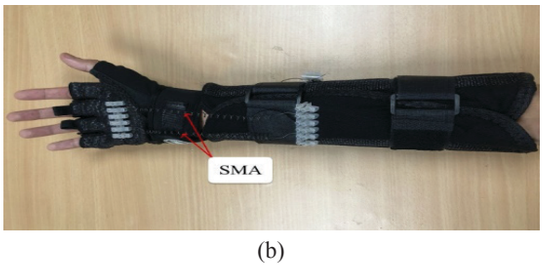

(b)

FIGURE 8. a) Top and b) bottom side of the wrist assistive device prototype

The prototype incorporates a glove and an arm splint, both equipped with straps to ensure they remain securely fastened to the hand, preventing any unwanted movement (Fig. 8). To achieve targeted actuation, four terminal blocks are secured with stitches at four locations: one slightly below the knuckles on the upper side of the arm (with the palm facing down), one on the arm itself (palm facing down), one at the center of the palm, and one on the arm (palm facing up). These terminal blocks serve as anchor points for the four SMA spring actuators used in the prototype. Two SMAs are secured to the terminal blocks on the top side of the arm, and the other two SMAs are attached to the blocks on the bottom side of the arm, ensuring balanced distribution of force. The SMAs are connected electrically in series to ensure the same amount of current is delivered for actuation consistency. The specifications of the SMA springs used in this study are presented in Table 3.

TABLE 3. SMA Spring (Nexmetal Corp.) specifications

Parameter	Value
Activation temperature	45-60°C
Wire diameter	0.75 mm
Spring outer diameter	6.6 mm
Spring free length	16 mm
Spring solid length	50 mm
Spring index	7.7

To achieve the intended wrist motion, the SMA actuators are placed at different sections on the arm to create the required force (torque) for the wrist ROM targeted as found from simulation studies. The placement and configuration of the actuators are illustrated in Figure 9. The approach taken to produce the four wrist motions independently involves supplying power to the SMA actuators in pairs. For example, to achieve extension (Mode 1), power is supplied to the two SMAs on the top side f the arm. Conversely, for flexion (Mode 2), power is applied to the two SMAs on the bottom side of the arm. For radial deviation (Mode 3), power is directed to the left SMA on the top side and the right SMA on the bottom side. Finally, for ulnar deviation (Mode 4), power is supplied to the right SMA on the top side and the left SMA on the bottom side. This targeted powering strategy is to generate appropriate torque for the intended wrist movement.

PERFORMANCE MEASUREMENT

TORQUE GENERATION

To determine the torque produced by the prototype, the force exerted by the SMA actuators embedded on the exoskeleton will be measured. The method for measuring torque is illustrated in Fig. 10, which consists of a force gauge (ZP-100N), a string, and a retort stand with clamps to ensure secure and stable positioning. A variable power supply is used to deliver 2A of current and 5V of voltage to the SMAs. For each of the targeted wrist motions which are extension, flexion, radial deviation, and ulnar deviation force measurements are recorded over a one-minute duration. These maximum forces enable the calculation of the maximum torque using the formula Torque = Force x Length, where length is the distance between wrist joint and force normal to the palm, measured as 6cm.

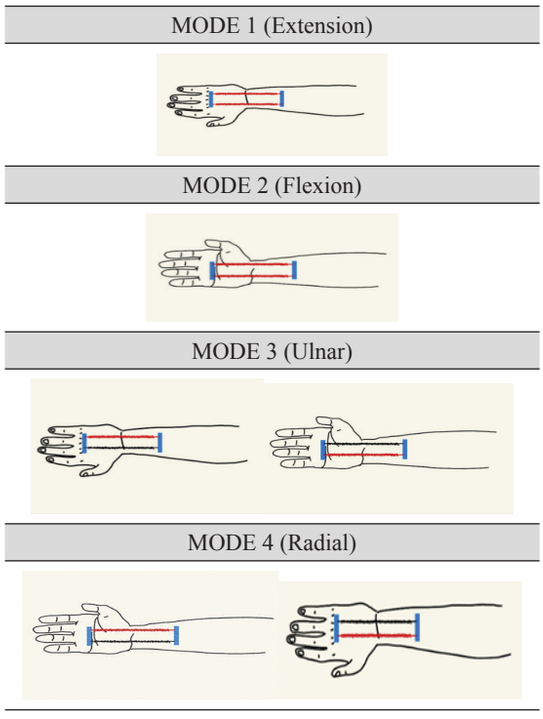

FIGURE 9. The SMA coil pair activated (red-heated, black-unheated) to achieve different wrist modes

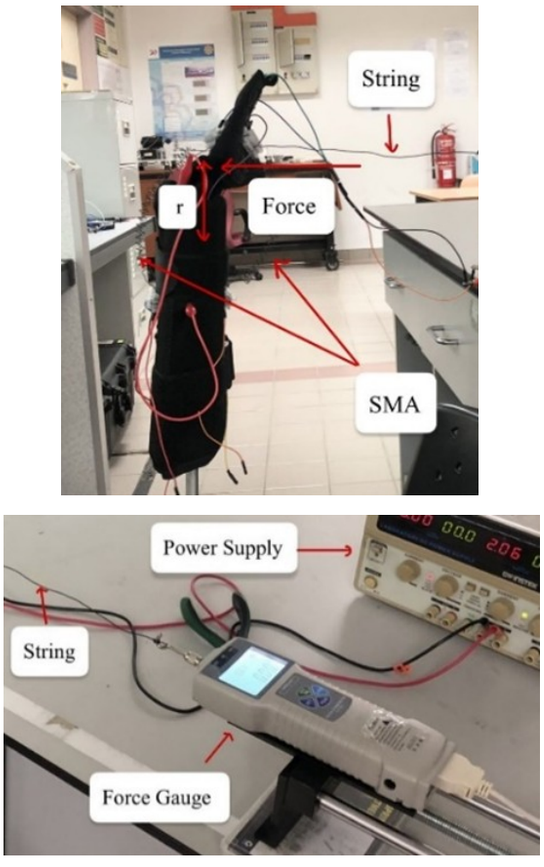

FIGURE 10. Detailed setup for torque measurement process

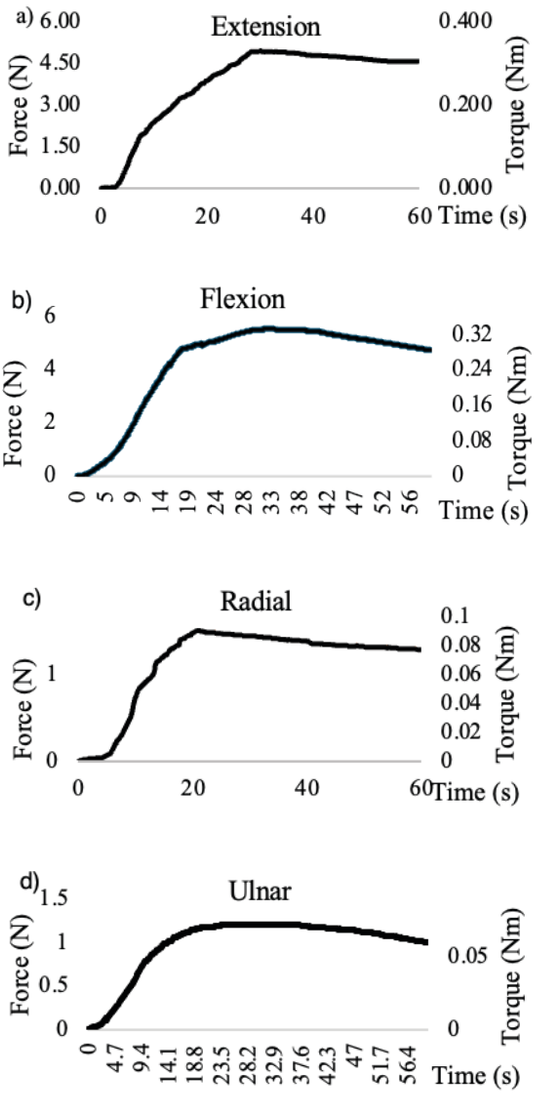

FIGURE 11. Experimental result for torque and force generated by SMA spring in a) extension (Mode 1), b) flexion (Mode 2), c) radial (Mode 3) and d) ulnar (Mode 4)

Figure 11 shows that the SMA spring actuators produced maximum torques of 0.328 Nm and 0.332 Nm during extension and flexion, respectively, after about 30 seconds of actuation. These values exceed the simulated requirements of 0.27 Nm for extension and 0.26 Nm for flexion, demonstrating that the actuator configuration is sufficient to support these motions effectively. For radial and ulnar deviations, the prototype exhibited lower torque outputs that did not meet the estimated requirement of 0.32 Nm. In terms of speed, all modes achieved the maximum torque at around 20 seconds.

The deficit torque generation in radial/ulnar modes may be attributed to the increased friction between the SMA actuators and the glove material during sideward wrist movements, which may prevent effective force

transmission. Another contributing factor could be the mechanical configuration of the SMA placements. Unlike extension and flexion, which benefit from direct and opposing actuator alignment along the wrist's vertical axis, the radial and ulnar deviations rely on diagonal actuation paths. A more effective configuration would involve positioning the SMAs along the sides of the palm i.e. aligning them along the thumb for radial deviation and along the little finger for ulnar deviation. This lateral placement would increase the moment arm, thereby enhancing torque output for these motions.

ACTUATION SPEED

The actuation speed of the prototype in one cycle is further measured to assess the feasibility of the prototype. The method for measuring the speed of actuation is depicted in Figure 12 where the wrist part is left free to move in extension-flexion pairs. The setup includes the MPU6050 sensor to measure the tilt angle, an Arduino Uno, and a variable power supply providing 2A of current and 5V of voltage to the SMA actuators. The speed of actuation is determined by the time taken to reach the peak angle of the first motion (extension) before transitioning to the second motion (flexion), following the alternating powering strategy as depicted in Figure 9 for Mode 1 and 2. The operational frequency of the SMA actuator can be calculated using (Nizamani et al. 2017):

$$f_w = \frac{1}{t_h + t_C} \tag{9}$$

where f_w is the operational frequency, t_h is heating time and t_C is cooling time of the SMA actuator.

Figure 13 shows the angle measured for extension and flexion mode. The upper region of the graph represents extension mode, and the lower region of the graph represents flexion mode. The red and blue region refers to when the SMA pairs for the Modes are heated and cooled, respectively.

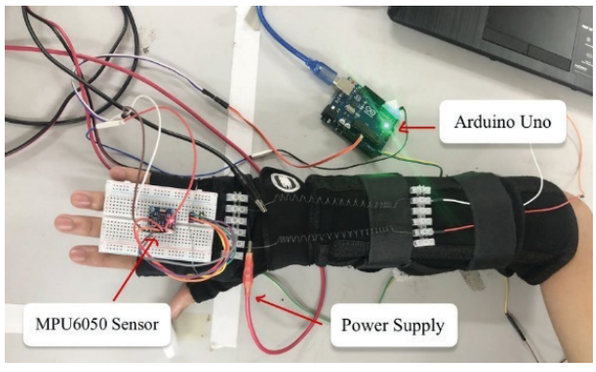

FIGURE 12. Detailed setup for actuation speed measurement process

During cooling phase for one of the modes, the SMA pair of the other mode is actuated to create a biased force to overcome the residual stress and helps restore the original position more rapidly. This is illustrated from the asymmetrical response times during heating and cooling phases as shown in Figure 13. The wrist motion reaches the extension peak (about 35°) from initial position at approximately 25s, returns back to 0° in 15s, reaches flexion maximum (about -35°) in about 14s, and returns back to 0° in 10s. The total cycle time for complete extension-flexion motion is around 1 min. The operational frequency for the SMA for Mode 1 and 2, and for one complete extension-flexion cycle is tabulated in Table 4.

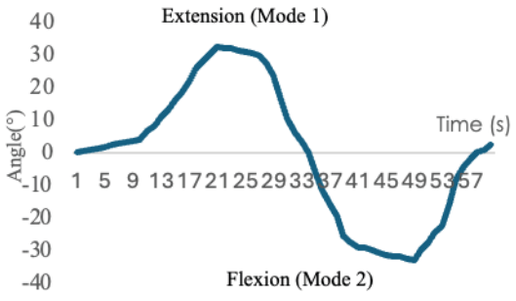

FIGURE 13. Angle vs. time (red-heating phase, blue-cooling phase)

TABLE 4. Operational frequency from experiment studies

Motion	Frequency
Extension	0.03Hz
Flexion	0.05Hz
One cycle	0.018Hz

The operational frequencies recorded for the extension (0.03 Hz) and flexion (0.05 Hz) motions indicate a relatively slow actuation speed, which is typical for SMA-based systems due to their inherent thermal response characteristics. The total cycle frequency of 0.018 Hz is obtained for one full extension-flexion cycle. The faster reversal motion (flexion) is aided by the antagonistic actuation mechanism, where the opposing SMA pair is activated to generate a bias force that facilitates faster return to the neutral position (0°). This highlights the advantage of the bidirectional SMA configuration in improving SMA actuator speed during the cooling phase. However, the heating phase remains the limiting factor due to the thermal inertia of the SMA material, suggesting a need for design improvements. Enhancements such as cooling via forced convection, using lower-volume SMA actuators, or SMA materials with faster transition temperature could significantly increase the actuation frequency.

CONCLUSION

This study presented the design, modelling, and experimental evaluation of a wrist exoskeleton prototype actuated by Shape Memory Alloy (SMA) springs to assist with flexion-extension and radial-ulnar deviation motions. Simulation results showed that the required torque for typical wrist rehabilitation motions ranges between 0.26–0.32 Nm. The developed prototype successfully generated torque values exceeding simulation requirements for flexion (0.332 Nm) and extension (0.328 Nm). However, the torques generated for radial and ulnar deviation modes are insufficient, likely due to actuator placement and increased friction. The faster reversal motion (from extension to flexion) was enabled by the biasing effect of the opposing SMA, while the slower heating phase was attributed to the low heat transfer rate to the SMA spring actuators

For future improvement, it is recommended to optimize the placement of SMA actuators, particularly for lateral wrist movements, to increase the moment arm and reduce friction. Actuation speed could be enhanced through active cooling strategies, reduced SMA thermal mass by using lower volume material, or higher heating rate such as pulsed high-current input. Overall, the SMA-based wrist exoskeleton shows strong potential as a lightweight wearable solution for various applications requiring compact actuators like exoskeleton.

ACKNOWLEDGEMENT

This research was supported by Ministry of Higher Education (MOHE) through Fundamental Research Grant Scheme (FRGS/1/2023/TK10/UIAM/02/3)

DECLARATION OF COMPETING INTEREST

None.

REFERENCES

Ali, H.F. & Kim, Y. 2023. Novel bio-inspired artificial muscle using shape memory alloy wire in spiral winding. *23rd International Conference on Control, Automation and Systems (ICCAS) 2023*: 1169–1173.

Fischer, G., Jermann, D., List, R., Reissner, L. & Calcagni, M. 2020. Development and application of a motion analysis protocol for the kinematic evaluation of basic and functional hand and finger movements using motion capture in a clinical setting – A repeatability study. *Applied Sciences (Switzerland)* 10(18). https://doi.org/10.3390/APP10186436

Garcia, G.F., Gonçalves, R.S. & Carbone, G. 2024. A review of wrist rehabilitation robots and highlights needed for new devices. *Machines* 12(5): 315.

Hamid, Q.Y., Hasan, W.W., Hanim, M.A., Nuraini, A.A., Hamidon, M.N. & Ramli, H.R. 2023. Shape memory alloys actuated upper limb devices: A review. *Sensors and Actuators Reports* 5: 100160.

Hope, J. & McDaid, A. 2017. Development of wearable wrist and forearm exoskeleton with shape memory alloy actuators. *Journal of Intelligent and Robotic Systems* 86(3–4): 397–417. https://doi.org/10.1007/s10846-016-0456-7

Jeong, J., Bin Yasir, I., Han, J., Park, C.H., Bok, S.K. & Kyung, K.U. 2019. Design of shape memory alloy-based soft wearable robot for assisting wrist motion. *Applied Sciences (Switzerland)* 9(19). https://doi.org/10.3390/app9194025

Jia, Z., Han, G., Jin, H., Xu, M. & Dong, E. 2024. Design and force/angle independent control of a bionic mechanical ankle based on an artificial muscle matrix. *Biomimetics* 9(1). https://doi.org/10.3390/biomimetics9010038

Krebs, H.I., Volpe, B.T., Williams, D., Celestino, J., Charles, S.K., Lynch, D. & Hogan, N. 2007. Robot-aided neurorehabilitation: A robot for wrist rehabilitation. *IEEE Transactions on Neural Systems and Rehabilitation Engineering* 15(3): 327–335.

Mayetin, U. & Kucuk, S. 2021. A low-cost 3-DOF force sensing unit design for wrist rehabilitation robots. *Mechatronics* 78: 102623.

Nexmetal Corp. Nitinol springs. https://nexmetal.com/collections/nitinol-springs/

Nizamani, A.M., Jawaid, D. & Nizaman, M.A.N. 2017. Development of faster SMA actuators. Dalam *Shape Memory Alloys – Fundamentals and Applications*. InTech. doi:10.5772/intechopen.69868

Park, C.H., Choi, K.J. & Son, Y.S. 2020. Shape memory alloy-based spring bundle actuator controlled by water temperature. *IEEE/ASME Transactions on Mechatronics* 24(4): 1798–1807. https://doi.org/10.1109/TMECH.2019.2928881

Park, S.J., Kim, U. & Park, C.H. 2020. A novel fabric muscle based on shape memory alloy springs. *Soft Robotics* 7(3): 321–331. https://doi.org/10.1089/soro.2018.0107

Perrelli, M., Lago, F., Garofalo, S., Bruno, L., Mundo, D. & Carbone, G. 2024. A critical review and systematic design approach for innovative upper-limb rehabilitation devices. *Robotics and Autonomous Systems*: 104835.

Pittaccio, S. & Viscuso, S. 2012. Shape memory actuators for medical rehabilitation and neuroscience. Dalam *Smart Actuation and Sensing Systems – Recent Advances and Future Challenges*. InTech. doi:10.5772/50201

Pitzalis, R.F., Park, D., Caldwell, D.G., Berselli, G. & Ortiz, J. 2023. State of the art in wearable wrist exoskeletons Part I: Background needs and design requirements. *Machines* 11(4): 458. https://doi.org/10.3390/machines11040458

Simone, F., Rizzello, G., Seelecke, S. & Motzki, P. 2020. A soft five-fingered hand actuated by shape memory alloy wires: Design, manufacturing, and evaluation. *Frontiers in Robotics and AI* 7. https://doi.org/10.3389/frobt.2020.608841

Serbest, K., Cilli, M. & Eldogan, O. 2018. A dynamic virtual hand model for estimating joint torques during wrist and finger movements. *Journal of Engineering Science and Technology* 13(6): 1665–1676.

Serrano, D., Copaci, D.S., Moreno, L. & Blanco, D. 2018. SMA-based wrist exoskeleton for rehabilitation therapy. Dalam *Proceedings of the IEEE/RSJ International Conference on Intelligent Robots and Systems (IROS) 2018*, Madrid, Spain: 2318–2323.

Su, Y.Y., Yu, Y.L., Lin, C.H. & Lan, C.C. 2019. A compact wrist rehabilitation robot with accurate force/stiffness control and misalignment adaptation. *International Journal of Intelligent Robotics and Applications* 3: 45–58.

Tang, T., Zhang, D., Xie, T. & Zhu, X. 2013. An exoskeleton system for hand rehabilitation driven by shape memory alloy. *IEEE International Conference on Robotics and Biomimetics (ROBIO) 2013*: 756–761.

Thomas, S.J., Zeni, J.A. & Winter, D.A. 2022. *Winter's Biomechanics and Motor Control of Human Movement*. John Wiley & Sons.

Villena Prado, G. & Castro Sanchez, M.B. 2019. Control strategy of a pneumatic artificial muscle for an exoskeleton application. *IFAC-PapersOnLine* 52(1): 281–286. https://doi.org/10.1016/j.ifacol.2019.06.075

Wang, Y. & Xu, Q. 2021. Design and testing of a soft parallel robot based on pneumatic artificial muscles for wrist rehabilitation. *Scientific Reports* 11(1): 1273.

Yeem, S., Heo, J., Kim, H. & Kwon, Y. 2019. Technical analysis of exoskeleton robot. *World Journal of Engineering and Technology* 7(1): 68–79. https://doi.org/10.4236/wjet.2019.71004

Zhang, L., Li, J., Cui, Y., Dong, M., Fang, B. & Zhang, P. 2020. Design and performance analysis of a parallel wrist rehabilitation robot (PWRR). *Robotics and Autonomous Systems* 125: 103390.